Phospholamban Pentamer Quaternary Conformation Determined by In-Gel Fluorescence Anisotropy[†,‡]

Seth L. Robia, Nicole C. Flohr, and David D. Thomas*

Department of Biochemistry, Molecular Biology, and Biophysics, University of Minnesota, Minneapolis, Minnesota 55455

Received October 6, 2004; Revised Manuscript Received December 14, 2004

ABSTRACT: We measured in-gel fluorescence anisotropy of phospholamban (PLB) labeled with the biarsenical fluorophore FlAsH at three different sites on the cytoplasmic domain. The 6 kDa monomer bands of FlAsH-tetracysPLB showed high anisotropy ($r = 0.29$), reflecting null homotransfer and low mobility ($S = 0.85$) on the nanosecond time scale of the FlAsH fluorescence lifetime. 30 kDa bands (pentameric PLB) within the same lanes exhibited low anisotropy, suggesting intrapentameric fluorescence energy homotransfer between PLB subunits. FlAsH labels positioned at residue −6, 5, or 23 showed a graduated pattern of fluorescence depolarization corresponding to resonance energy transfer radii of 46 ± 2, 38 ± 4, and <25 Å, respectively. Pentamer anisotropy increased with heating or fluorescence photobleaching toward a maximum value similar to that determined for monomeric PLB. Fluorescence resonance energy heterotransfer was also observed in vitro and in vivo within PLB pentamers colabeled with FlAsH and the biarsenical fluorophore ReAsH. In vitro heterotransfer efficiencies were graduated by labeling position, in harmony with homotransfer results. The calculated transfer radii compare favorably to distances predicted by a computer molecular model of the phospholamban pentamer constructed from NMR solution structures. The data support a helical pinwheel model for the PLB pentamer, in which the cytoplasmic domains bend sharply outward from the central bundle of helices.

On a cellular level, the cardiac cycle is orchestrated by release of calcium into the cytosol during systole (contraction) and subsequent reuptake of calcium into internal stores by an ion-motive ATPase during diastole (relaxation). This pump, the sarco(endo)plasmic reticulum calcium ATPase (SERCA),[1] is tightly regulated to appropriately meet the varying demands of stress and rest. In the absence of β-adrenergic stimulation, the apparent calcium affinity of SERCA is reduced by an inhibitory interaction with a 52-amino acid transmembrane protein, phospholamban (PLB) (*1*, *2*). Activation of β-adrenergic pathways culminates in phosphorylation of PLB by cAMP-dependent protein kinase (PKA) or calmodulin-dependent protein kinase (*3*−*5*), relieving inhibition of the pump. Disorders of cardiac SERCA regulation are associated with heart failure (*6*, *7*). In particular, ablation (*8*) or point mutation (*9*) of PLB results in dilated cardiomyopathy and heart failure in humans. Conversely, gene delivery of a pseudophosphorylated mutant PLB prevented progression to heart failure in a cardiomyopathic hamster model (*10*). Thus, phospholamban is an attractive target for therapeutic interventions in the treatment of heart failure (*9*), a leading cause of death in the United States (*11*) and other developed countries.

An interesting feature of phospholamban is its propensity for oligomerization into homopentamers (*12*). These structures are stabilized by Leu/Ile zipper interactions between transmembrane residues (*13*−*16*) and are SDS-resistant, allowing resolution of pentamer, monomer, and intermediate-order oligomers by SDS−polyacrylamide gel electrophoresis (*17*, *18*). While the physiological role of the pentamers is uncertain, disrupting pentamer formation by mutagenesis results in superinhibition of the pump (*19*, *20*, *37*), with consequent pathology in vivo (*21*). These results, along with spectroscopic studies (*22*, *23*), suggest that the monomeric form of PLB is the major inhibitory species. It has been suggested that the pentameric species represents a reserve pool of reduced activity in dynamic equilibrium with the monomer (*24*). Phosphorylation of PLB may alter this equilibrium (*22*) and change the quaternary conformation of the pentamer (*4*). Several disparate models have been proposed for the conformation of the PLB pentamer (Figure 1A). Smith and co-workers have provided solid state NMR and FT-IR evidence for a highly α-helical PLB oriented perpendicular to the membrane plane (*25*, *26*). This implies a fully coiled-coil pentamer structure, depicted schematically in part 1 of Figure 1A. In contrast, a solution NMR study of residues 1−36 supports a model of two α-helical regions joined by a flexible hinge (*27*), which would allow axial

[†] This work was supported by a grant to D.D.T. from the National Institutes of Health (GM27906). S.L.R. was supported by a postdoctoral fellowship from the American Heart Association (0320022Z).

[‡] A structural model of the phospholamban pentamer has been deposited with the Protein Data Bank (entry 1XNU).

* To whom correspondence should be addressed. E-mail: ddt@umn.edu. Phone: (612) 625-0957. Fax: (612) 624-0632.

[1] Abbreviations: βME, 2-mercaptoethanol; BSA, bovine serum albumin; DTT, dithiothreitol; EDT, ethanedithiol; FITC, fluorescein isothiocyanate; FlAsH, fluorescein arsenical helix/hairpin binder; FRET, fluorescence resonance energy transfer; HEPES, *N*-(2-hydroxyethyl)-piperazine-*N*′-2-ethanesulfonic acid; PAGE, polyacrylamide gel electrophoresis; PLB, phospholamban; ReAsH, resorufin arsenical helix/hairpin binder; ROI, region of interest; SDS, sodium dodecyl sulfate; SERCA, sarco(endo)plasmic reticulum calcium adenosine triphosphatase; TCEP, tris(2-carboxyethyl)phosphine; WT, wild-type.

10.1021/bi0478446 CCC: $30.25
Published on Web 02/25/2005

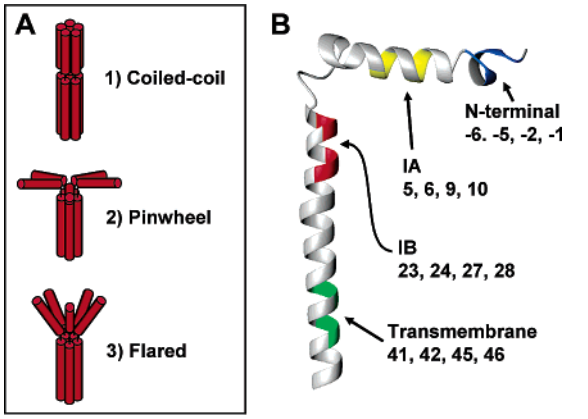

FIGURE 1: (A) Models of PLB quaternary conformation: coiled coil (*25*), helical pinwheel (*27*), and flared (*4*). (B) Tetracysteine repeats created on phospholamban for derivatization with biarsenical fluorophores.

declination of the cytoplasmic domain toward the surface of the membrane (part 2 of Figure 1A). Intermediates between these two extremes are also possible (part 3 of Figure 1A). Jones and colleagues speculated that charge repulsion caused flaring of PLB cytoplasmic domains, and that this electrostatic conformational effect might vary with phosphorylation (*4*, *28*).

It is possible that the detergent used in this study to solubilize the membrane protein phospholamban affects its structure. A previous study from our lab showed a decreased intrapentameric probe separation distance in SDS compared to lipid vesicles (*23*). However, this observation is complicated by the use of fluorescent dyes with long (>10 Å) linkages to PLB, a mixed population of monomers and pentamers, and the existence of large aggregates of 9−11 PLB subunits in that preparation (*23*). In this study, we avoid these complications by the use of a short linkage bidentate dye and by physically resolving monomers and higher-order aggregates from pentameric PLB, the major native oligomeric species. Phospholamban has essentially the same oligomeric stability in SDS as in lipid membranes (*22*) and retains high thermal stability of the oligomer (*12*). In SDS solution, PLB displays phosphorylation-sensitive intrinsic fluorescence (*29*), PKA- and CAMKII-dependent gel mobility shifts (*30*) in excess of the expected change in molecular weight, and a high helical content (*29*, *31*) that is similar to its helical content in lipid (*32*). Taken together, these previous studies suggest that phospholamban secondary structure and quaternary interactions are intact in the presence of SDS.

Site-directed labeling of each of several positions along the PLB cytoplasmic domain (Figure 1B) with biarsenical fluorophores (*33*, *34*) offers an improvement in structural resolution over previous studies that labeled PLB at Lys3 (*23*, *24*). Determination of the relative dispositions of PLB cytoplasmic domains allows us to discriminate among models of pentamer quaternary conformation.

MATERIALS AND METHODS

Tetracysteine Mutagenesis of Phospholamban. Site-directed mutagenesis of plasmid pGEX-PLB (WT canine PLB on a pGEX-KT backbone) (*35*) was performed with the QuikChange mutagenesis kit (Stratagene, La Jolla, CA) to create tetracysteine motifs suitable for derivatization. For constructs 1A-tetracysPLB, 1B-tetracysPLB, and TM-tetracysPLB, cysteines were substituted for four endogenous residues, retaining two native residues in the intervening sequence. Construct N-term-tetracysPLB was a seven-residue addition preceding the native N-terminal methionine. The optimal FlAsH-binding sequence has a proline-glycine intervening sequence between the pairs of cysteines (*36*). We used this motif for the N-term-tetracysPLB construct. In the interest of minimizing changes to PLB, all other constructs retained the native residues at the positions corresponding to the intervening sequence. Oligonucleotide mutagenic primers are listed in Table 1. For construct 1B-tetracysPLB, simultaneous introduction of the entire tetracysteine repeat proceeded with poor efficiency, so cysteine codons were introduced pairwise. Construct N-term-tetracysPLB was engineered by conventional recombinant PCR, using flanking oligos that encoded 5′ BamHI and 3′ EcoRI sites (Table 1). These restriction sites were used to insert the amplified N-term-tetracysPLB cDNA into pGEX-KT. TetracysPLB-encoding cDNA clones were gel purified, subcloned into a baculoviral shuttle vector pVL-1393, and transformed into *Escherichia coli*. Plasmid DNA was prepared from 40 mL cultures by Qiagen MidiPrep (Valencia, CA), and clones were confirmed by sequencing.

Baculovirus/SF9 Insect Cell Expression of TetracysPLB. Insect cells were cultured and coinfected with baculovirus and pVL-1393 using the BaculoGold Transfection System (BD Biosciences, San Diego, CA) according to manufacturer's instructions. Recombinant viruses were amplified by successive rounds of infection, and tetracysPLB proteins were expressed at 27 °C for 4 days (*37*). Protein expression was verified by Western blotting with mAb 8A3-D5 (*38*) and 1D11 (*39*). For construct IA-tetracysPLB, which was unreactive to 8A3-D5 and 1D11, expression was inferred from the presence of FlAsH-reactive bands corresponding to the known mobilities of the phospholamban monomer and pentamer on SDS−polyacrylamide gels of IA-tetracysPLB insect cell homogenates. Relative expression of PLB variants was also evaluated with a fluorescent general protein gel stain SYPRO Ruby (Molecular Probes, Eugene, OR). SYPRO-stained gels were quantified with a STORM phosphorimager (Molecular Dynamics, Sunnyvale, CA).

Preparation of Insect Cell Homogenates and Microsomes. Insect cells expressing recombinant phospholamban were pelleted by centrifugation at 400*g* and disrupted with a tissue homogenizer (Tekmar, Cincinnati, OH) in 250 mM sucrose and 30 mM histidine (pH 7.5). Microsomes containing wild-type or tetracysPLB protein were prepared by Parr bomb, as previously described (*16*).

FITC Labeling of PLB and BSA. Labeling of BSA with FITC was accomplished by incubation of 1 mg/mL BSA with 1.5−375 μM FITC in PBS (pH 8.0) overnight at 20 °C with stirring. WT PLB microsomes were dialyzed against PBS (pH 8.0) to remove amine-containing buffer, and then incubated with 10 or 200 μM FITC for 2 h at 20 °C.

Labeling of TetracysPLB with ReAsH/FlAsH. To ensure that cysteines were in a reduced form suitable for derivatization by biarsenicals (*36*), insect cell homogenates or microsome preparations containing tetracysPLB were incubated overnight at 20 °C in a buffer of 100 mM NaCl, 2% SDS, 1 mM β-mercaptoethanol (βME), 1 mM tris(2-carboxyethyl)phosphine hydrochloride (TCEP), 1 mM dithio-

Table 1: Oligonucleotide Primers for Tetracysteine Mutagenesis

primer name	primer sequence	"tetracysPLB construct" AA sequence, primer direction
SLR#11	AAGGATCCATGTGTTGTCCTGGGTGTTGTATGGATAAAGTCCAATACCTC	N-term MCCPGCCMDK..., forward
SLR#14	AAGAATTCTCAGAGAAGCATCACAATGAT	N-term MCCPGCCMDK..., reverse
SLR#19	GGATAAAGTCTGCTGCCTCACTTGCTGCGCTATTAGAAGAGCTTCAACC	IA ...KVCCLTCCAI..., forward
SLR#20	GGTTGAAGCTCTTCTAATAGCGCAGCAAGTGAGGCAGCAGACTTTATCC	IA ...KVCCLTCCAI..., reverse
SLR#9	ACCATTGAAATGCCTCAATGTTGTCGTCAAAATCTTCAGAACCTA	step 1, IB ...PQCCRQNLQN..., forward
SLR#10	TAGGTTCTGAAGATTTTGACGACAACATTGAGGCATTTCAATGGT	step 1, IB ...PQCCRQNLQN..., reverse
SLR#21	CCTCAATGCTGCCGTCAATGCTGCCAGAACCTATTTATAAATTTCTG	step 2, IB ...PQCCRQCCQN..., forward
SLR#22	CAGAAATTTATAAATAGGTTCTGGCAGCATTGACGGCAGCATTGAGG	step 2, IB ...PQCCRQCCQN..., reverse
SLR#5	TGTCTCATTTTAATATGTTGTTTGTTGTGTTGCATCATTGTG	TM ...LICCLLCCII..., forward
SLR#6	CACAATGATGCAACACAACAAACAACATATTAAAATGAGACA	TM ...LICCLLCCII..., reverse

threitol (DTT), 15 μM ethanedithiol (EDT), and 50 mM HEPES (pH 8.0). After overnight reduction, ReAsH−EDT_2 and/or FlAsH−EDT_2 (Invitrogen, Carlsbad, CA) was added to a final concentration of 1−50 μM, and the labeling reaction was allowed to proceed for 12 h at 20 °C. We obtained the most reliable results by performing reduction and labeling under nitrogen.

In-Gel Fluorescence Macroscopy. Labeled samples were mixed 1:1 with Laemmli sample buffer and subjected to polyacrylamide gel electrophoresis with Ready Gel 15% Tris-HCl (Bio-Rad, Hercules, CA). Polarization macroscopy to measure fluorescence anisotropy was accomplished by illumination of the gel with a xenon lamp equipped with a horizontally oriented polarizer filter and a 470/40 chromatic filter. Fluorescence emission was collected through a 515LP chromatic filter and a rotatable polarizing filter that was positioned in either a parallel or perpendicular configuration with respect to the polarization of the excitation light. Gel images were integrated with a Sensys 12 bit CCD camera (Photometrics, Tucson, AZ) mounted 40 cm above the gel. Successive images of a gel acquired with the analyzing polarizer in parallel and perpendicular configurations were aligned in a stack using the public domain software ImageJ. The CCD detector was equally sensitive to X- and Y-polarized emission (G-factor = 1). Each band was manually circumscribed to define a region of interest (ROI), and the fluorescence emission intensity was integrated over the area of the band. Integrated ROI volumes were background corrected using neighboring empty lanes (containing no fluorescent sample) as paired references. Fluorescence anisotropy was calculated by comparing the integrated ROI volumes of the parallel and perpendicular images according to the relationship $(I_{para}/I_{perp} - 1)/(I_{para}/I_{perp} + 2)$. To create a graphical representation of the anisotropy of the polyacrylamide gel, a dichroic ratio image of parallel to perpendicular was generated with ImageJ, and transformed according to the relationship given above. To measure the fluorescence anisotropy of proteins derivatized with FITC, gels were soaked in 100% glycerol for 30 min prior to imaging. This eliminated probe rotational mobility as a source of fluorescence depolarization. Heterotransfer FRET in FlAsH/ReAsH colabeled pentamer bands was evaluated by removing excitation and emission polarizing filters, and replacing the emission chromatic filter with a 510/20 band-pass filter selective for FlAsH fluorescence.

Photobleaching Tests of FlAsH−FlAsH HomoFRET and FlAsH−ReAsH HeteroFRET. Protein bands of interest were excised from polyacrylamide gels using a razor blade and transferred to a quartz sub-micro fluorometer cell with a nominal volume of 50 μL containing SDS−PAGE running buffer. For FlAsH photobleaching, the sample was placed in an ISS-K2 polarizing fluorometer (ISS, Champaign, IL) and illuminated with the 498.5 nm line of an argon laser (Coherent, Santa Clara, CA) at 10 mW of output power. Sample fluorescence emission intensity and anisotropy were continuously monitored during bleaching. Care was taken to operate within the dynamic range of the equipment by attenuating emitted light before it reached the photomultiplier tube. The pentamer band of SDS−polyacrylamide gels of FlAsH/ReAsH colabeled samples was excised as described above, and its fluorescence emission spectrum was obtained. For selective photobleaching of ReAsH, the gel slice was illuminated with the 568 nm line of a Kr/Ar mixed gas laser (Bio-Rad) at maximum output (estimated power of 10 mW). At intervals, the cuvette was transferred to the fluorimeter to obtain a series of postbleaching emission spectra.

In Vivo Confocal Imaging of FlAsH/ReAsH Labeled Phospholamban. Adherent Sf21 insect cells expressing IB-tetracysPLB were incubated with 1 μM FlAsH, 2 μM ReAsH, 0.5 μM EDT, 1 mM βME, and 1 mM TCEP in Grace's Insect Medium supplemented with 10% fetal bovine serum. Cells were washed once, sloughed, and imaged with an upright Olympus AX-70 microscope equipped with a MRC 1024 Confocal laserhead, and a 60 × 1.40 NA Plan Apo objective. FlAsH was detected with 488 nm excitation and a 522 DF32 emission filter; ReAsH was detected with 568 nm excitation and a 605 DF32 emission filter. Selective ReAsH acceptor photobleaching was accomplished by increasing the scan zoom to 10×, and illuminating the sample with the 568 line of the Kr/Ar mixed gas laser at 100% intensity.

Heat Disruption of the PLB Pentamer. Pentamer bands excised from polyacrylamide gels were heated in a quartz cuvette by immersion in a boiling water bath, and transferred at intervals to a fluorometer for spectroscopy. Alternatively, the temperature was controlled directly using a custom-built cuvette holder equipped with a 2.5 Ω resistor through which was passed 2.5 A from a DC power supply. Spectroscopic measurements were acquired continuously during heating, and the temperature of the buffer solution covering the gel slice was monitored by a thermocouple and multimeter (ExTech Instruments, Waltham, MA).

Förster Distance (R_0) Calculation. The half-maximal fluorescence resonance energy transfer radii for heterotransfer (FlAsH to ReAsH) and homotransfer (FlAsH to FlAsH, FITC to FITC) processes were calculated according to the relationship $R_0 = 9790(J\kappa^2 n^{-4}\phi_D)^{1/6}$ (*40*), where ϕ_D is the donor quantum yield, J is the overlap integral, calculated from the

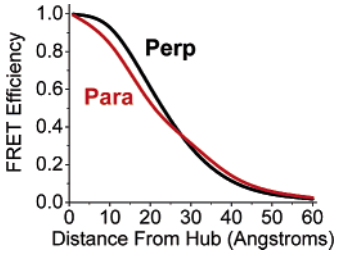

FIGURE 2: A simulation of PLB intrapentameric FRET efficiency for two possible attachments of FlAsH.

donor emission and acceptor absorbance spectra by the equation $J = \int f(\lambda)\epsilon(\lambda)\lambda^4\, d\lambda$ using a custom script running in Origin (Northampton, MA). κ^2 is the orientation factor, a function of the respective orientation of the donor emission and acceptor absorption transition moments according to the relationship $\kappa^2 = (\cos\theta_T - 3\cos\theta_D \cos\theta_A)^2$, where θ_T is the transfer angle, θ_D is the donor angle, and θ_A is the acceptor angle with respect to the vector joining the donor and acceptor dipoles. For analysis of homotransfer by the cluster theory method (*41*, *42*) described below, fluorescence dipole moments were assumed to have uncorrelated orientations ($\kappa^2 = {}^2/_3$). Alternatively, values of θ_T, θ_D, and θ_A were estimated from a geometric model of the phospholamban pentamer that examined several azimuthal (twist) angles and a range of axial (tilt) angles of the phospholamban cytoplasmic domains. For simplicity, PLB cytoplasmic domain α-helices were modeled as coplanar vectors with the FlAsH transition dipole considered either perpendicular to the axis of the cytoplasmic domain α-helix (*33*) and parallel to the membrane surface, or parallel to the domain (*43*). Briefly, probe separation distance d_F is determined by $2\sin(\alpha/2) \times (r_H + r_C)$, where α is the cytoplasmic domain azimuthal angle, r_H is the hub radius of the transmembrane domain coiled coil, and r_C is the radius of a circle precessed by the probe about the PLB transmembrane domain axis. The precession circle radius r_C is the product of $(d_L) \times \sin(\beta)$, where d_L is the distance of the probe from the cytoplasmic domain "hinge" and β is the phospholamban domain axial angle with respect to the membrane normal. The relative angle between two cytoplasmic domain helices is $2[\sin^{-1}(r_C/d_F/2)]$. This model demonstrates that although κ^2 for a given donor−acceptor pair varied considerably with α and β (data not shown), this factor had a relatively small impact on the total intrapentameric energy transfer efficiency. This was due in part to the much stronger dependence of FRET on the probe separation distance compared to κ^2, and the averaging of azimuthal orientations among an ensemble of cytoplasmic domains. This is evident in the simulated dependence of FRET on primary sequence labeling position using a set axial angle of 90° (Figure 2). FRET efficiency decreases as the probe is moved toward the N-terminus, and the uncertainty of FlAsH attachment (parallel vs perpendicular) (*33*, *43*) does not cause large errors. Fluorescein attached to PLB by a single covalent bond to Lys3 was assumed to have a random distribution of dipole orientations ($\kappa^2 = {}^2/_3$).

Scarlatta/Knox Model of the Relationship between Oligomerization and Cluster Anisotropy. It is sometimes desirable to use a single species of chromophore for FRET studies (*44*−*47*). This eliminates uncertainties involved with labeling PLB with multiple probe color variants directed to the same

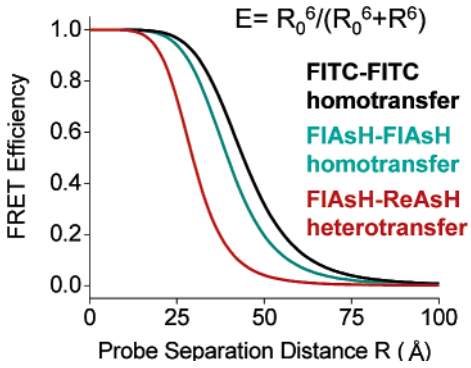

FIGURE 3: Simulated FRET efficiency as a function of probe separation for several pairs of fluorophores.

target sites. Because of overlap of a probe's emission spectrum with its own excitation spectrum, nonradiative energy transfer can occur between like fluorophores with high efficiency (Figure 3). Since the donor and acceptor are spectrally identical, homotransfer FRET is quantified by depolarization of the fluorescence emission. A cluster theory described by Knox (*42*) for homotransfer FRET in a complex was generalized by Runnels and Scarlatta (*41*) to approximate the relationship between intra-oligomeric fluorescence homotransfer and oligomer fluorescence anisotropy by the formula

$$r_n = r_1\frac{1 + (R_0/R)^6}{1 + N(R_0/R)^6} + r_{et}\frac{(N-1)(R_0/R)^6}{1 + N(R_0/R)^6}$$

where r_n is the fluorescence anisotropy of the oligomer, r_1 the emission anisotropy of the initially excited probe, R the probe separation distance, R_0 the Förster transfer radius, and N the number of subunits in the pentamer. r_{et} is the emission anisotropy of the probe excited by electronic energy transfer, which is assumed to be zero (*48*). In the case of substoichiometrically labeled phospholamban pentamers, the subunit number N depended upon the dye:protein ratio. For comparative analysis of data from experiments using different FlAsH labeling conditions (e.g., dye concentration), pentamer stoichiometries were calibrated to IB-tetracysPLB. Because the transfer distance R for this construct was below the range of transfer sensitivity (i.e., maximal FRET), its measured anisotropy r depended on only N.

Phospholamban Pentamer Molecular Modeling. Molecular models of pentameric phospholamban were constructed by superimposing individual frames of the NMR solution structures (*49*) transmembrane domain onto the corresponding backbone residues of the pentameric transmembrane domain model by Karim et al. (*15*). Homopentamers of the 20 frames of the NMR solution were energy minimized using the Discover engine of InsightII (*50*) and compared on the basis of their solvation free energy values. From the original 20 structures, 12 were eliminated as being unlikely due to atomic overlap of adjacent subunit cytoplasmic domains. Using a Delphi-based residue level solvation simulation, the electrostatic solvated conformational energies were calculated on each of the remaining eight pentamers to determine the lowest-energy structure. Separation distances between labeling sites on the 1A and 1B domains (Cys5, -6, -9, and -10 and Cys23, -24, -27, and -28, respectively) were determined from distances between the mean positions of tetra-Cys

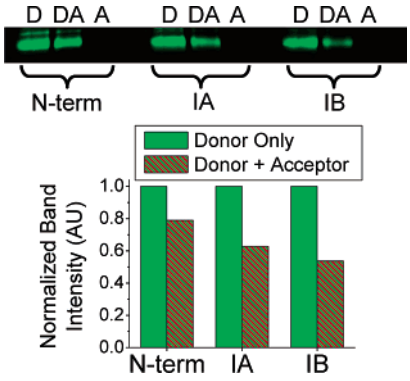

FIGURE 4: Several tetracysPLB variants labeled with donor (D), acceptor (A), or both (DA) showed a graduated pattern of quenching.

repeat α-carbons. In the absence of direct structural information about construct "N-term", the N-terminal tetra-Cys repeat was modeled as a two-residue helical extension plus a four-residue turn, a likely conformation for this proline-containing sequence. Intrapentameric transfer distances were measured from the mean position of the labeling site cysteine α-carbons. Molecular model figures were rendered with MOLMOL (*51*).

RESULTS

Heterotransfer FRET between FlAsH and ReAsH. Fluorescence imaging of a polyacrylamide gel of IB-tetracysPLB colabeled with either 1 μM FlAsH (donor, D), 1 μM ReAsH (acceptor, A), or both (DA) shows the green fluorescence emission of FlAsH in lanes D and DA (Figure 4, top panel). ReAsH (A) lanes appear dark, demonstrating band-pass filter selectivity for FlAsH fluorescence. Quantification of bands indicates samples labeled with both donor and acceptor (DA) are quenched in comparison to the donor only control (D) (Figure 4, bottom panel). Values are normalized to donor fluorescence. The observed quenching is partly due to competition between FlAsH and ReAsH for tetracysteine labeling sites, as well as FRET between FlAsH and ReAsH. Interestingly, there is a pattern of differential quenching for the different labeling sites examined. N-term quenched the least, followed by IA and IB. Excised pentamer bands of colabeled PLB were placed in a microcuvette and evaluated by fluorimetry. They showed emission spectrum peaks characteristic of FlAsH (green, $\lambda_{max} = 535$ nm) and ReAsH (red, $\lambda_{max} = 600$ nm) (Figure 5). The red emission decreased in response to selective photobleaching of ReAsH by 568 nm illumination from a Kr/Ar laser, with a concomitant increase in the green emission of FlAsH. This dequenching of the donor in response to selective photobleaching of the acceptor is indicative of fluorescence resonance energy transfer. Similarly, boiling a cuvette containing a gel slice of the colabeled pentamer band also resulted in enhancement of green FlAsH donor emission and decreased red ReAsH acceptor emission (Figure 6). This is consistent with loss of FlAsH−ReAsH heteroFRET due to dissociation of tetracys-PLB pentamers into monomers.

Intrapentameric FRET was also detected by confocal microscopy of live Sf21 insect cells expressing IB-tetracys-PLB colabeled with 1 μM FlAsH and 2 μM ReAsH (Figure 7). Green FlAsH fluorescence colocalized with red ReAsH fluorescence in the perinuclear region (probably the endo-

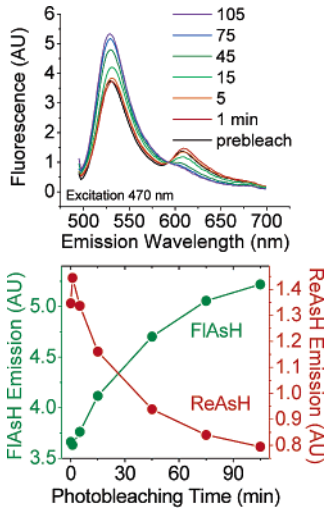

FIGURE 5: Selective photobleaching of the acceptor in FlAsH−ReAsH colabeled PLB.

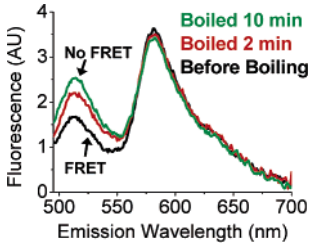

FIGURE 6: Heat disruption of PLB pentamers results in loss of FRET.

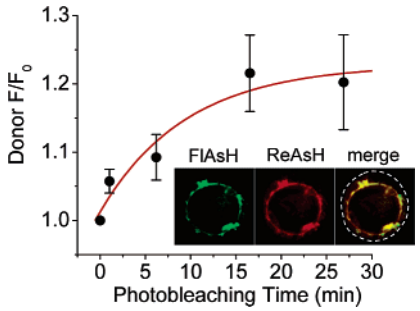

FIGURE 7: Selective photobleaching of the acceptor in insect cells colabeled with FlAsH−ReAsH results in increased donor (green) fluorescence detected by confocal microscopy. The inset shows that FlAsH (green) and ReAsH (red) fluorescence colocalize in the perinuclear region. The dotted perimeter indicates the cell margin.

plasmic reticulum), appearing yellow in the merged red−green overlay (Figure 7, inset). Selective acceptor photobleaching of ReAsH with 568 nm illumination results in a 20% increase in FlAsH emission over the course of 15 min (Figure 7). The values plotted in Figure 7 are mean F/F_0 values of the green emission channel (522/32 nm) ± the standard error (SE) for three experiments, and are described well by a single exponential ($\tau = 9.5$ min) (*52*). Control insect cells expressing wild-type phospholamban were also incubated with FlAsH and ReAsH. They showed a punctate, poorly colocalized distribution of red and green fluorescence, and did not exhibit donor dequenching by acceptor photobleaching (results not shown).

In-Gel Fluorescence Anisotropy of FITC−BSA. FITC-labeled BSA (FITC−BSA) subjected to SDS−PAGE resolved to an 85% homogeneous band visible by fluorescence macroscopy (Figure 8). FITC−BSA fluorescence anisotropy

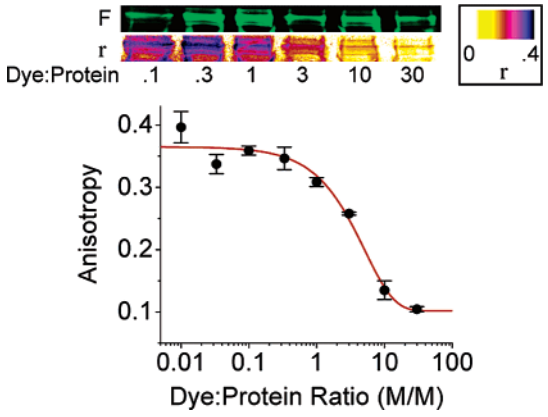

FIGURE 8: Polyacrylamide gel electrophoresis of FITC−BSA labeled at a range of dye:protein ratios, a fluorescence image (*F*), and an anisotropy image (*r*). Labeling at a high dye:protein ratio results in intramolecular homoFRET and decreased anisotropy.

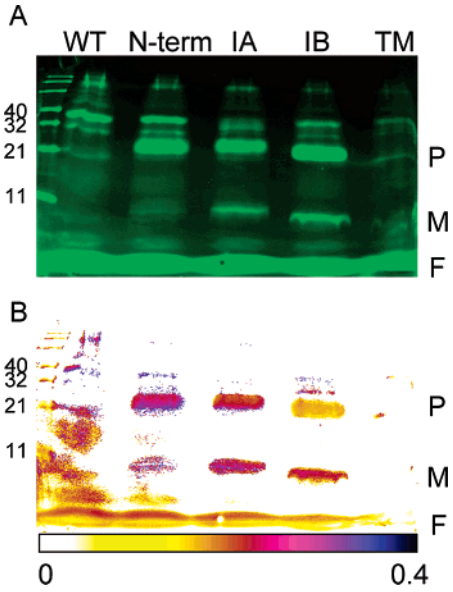

FIGURE 9: (A) Fluorescence intensity and (B) anisotropy (pseudocolor) images of FlAsH-tetracysPLB PAGE. The scale bar indicates the range of anisotropy values displayed.

was initially low due to the high rotational mobility of the fluorescein. After the gel had been soaked in 100% glycerol for 30 min, the fluorescence anisotropy of all FITC−BSA samples increased as a result of the increased solution viscosity, particularly for samples labeled with low dye:protein stoichiometry. Figure 8 shows the fluorescence (*F*) and anisotropy (*r*) images of FITC−BSA PAGE bands, demonstrating that anisotropy decreases as the applied dye:protein ratio increases. This is quantified in the bottom panel of Figure 8. Values are means ± the standard deviation (SD) of triplicate image sets. The anisotropy of FITC−BSA decreased as a sigmoid function of increasing dye:protein ratio to a minimum value of 0.1. This suggests an increasing level of homotransfer among fluorescein probes as BSA is progressively derivatized with additional fluorophores per protein macromolecule.

In-Gel Fluorescence Anisotropy of TetracysPLB Mutants Derivatized with FlAsH and FITC. FlAsH-labeled phospholamban was analyzed by SDS−polyacrylamide gel electrophoresis and in-gel polarization macroscopy. Figure 9 shows the fluorescence intensity (A) and anisotropy (B) images of FlAsH-labeled tetracysPLB variants. Monomeric and pentameric forms of N-term-, IA-, and IB-tetracysPLB are apparent, while WT-PLB and TM-tetracysPLB (containing a tetra-Cys repeat in the transmembrane domain) were unreactive to biarsenicals. Figure 9B demonstrates that monomer forms of all tetracysPLB mutants reported high fluorescence anisotropy consistent with null homotransfer and a probe attachment that was relatively rigid on the nanosecond time scale of the FlAsH fluorophore excited-state lifetime. While the free biarsenical dyes are reported to have a very low quantum yield (*36*), we detected free FlAsH fluorescence. Unincorporated dye was always very well resolved from proteins by electrophoresis, running as a dye front (F). Unincorporated FlAsH was freely mobile and exhibited low anisotropy. Interestingly, formation of the pentamer form of phospholamban resulted in a decrease in fluorescence anisotropy. The change in anisotropy due to pentamer formation varied with the position of the FlAsH label. IB-tetracysPLB, labeled near the clustered transmembrane helices, had the lowest anisotropy. As the labeling site was moved toward the N-terminus, the degree of depolarization decreased (anisotropy increased), suggesting a decreased amount of resonance energy transfer. The anisotropy values determined by fluorescence macroscopy are summarized in Figure 10.

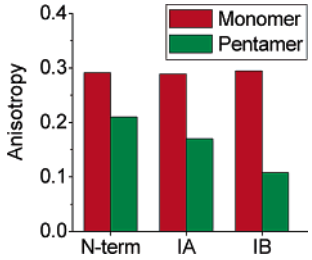

FIGURE 10: In-gel anisotropy measurements suggest the extent of FRET decreases as the tetra-Cys labeling site is moved toward the N-terminus.

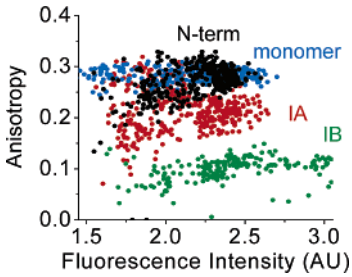

FIGURE 11: Fluorescence vs anisotropy for N-term-, IA-, and IB-tetracysPLB bands, and for monomeric PLB.

The fluorescence intensity within each tetracysPLB pentamer band was poorly correlated to the fluorescence anisotropy measured at that position. This is demonstrated in Figure 11, in which the calculated anisotropy values of sampled *r* image pixels are plotted against their paired fluorescence intensity values. There is no correlation between these intrinsic fluorescence signals, which argues against the observed pentamer fluorescence depolarization being due to random diffusion-enhanced FRET from concentration of the labeled protein in the pentamer band.

Wild-type phospholamban labeled with FITC on Lys3 was also analyzed by in-gel fluorescence anisotropy (Figure 12). Like that of FITC−BSA, its anisotropy before exposure to glycerol was low (0.15), reflecting the high mobility of the singly bound fluorophore (not shown). After the gel had been

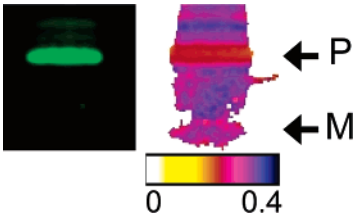

FIGURE 12: FITC-labeled WT-PLB in a glycerol-soaked polyacrylamide gel. The pentamer (P) showed reduced anisotropy compared to that of the monomer (M).

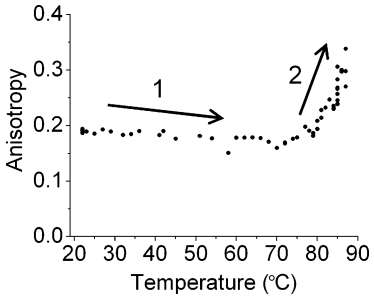

FIGURE 13: Heat disruption of FlAsH-labeled PLB pentamers results in increased anisotropy.

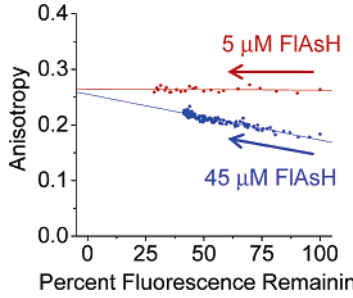

FIGURE 14: Progressive photobleaching of well-labeled FlAsH-tetracysPLB pentamers results in increased anisotropy (blue points).

soaked in 100% glycerol, the probe became immobilized, and the monomer form had a highly polarized emission ($r = 0.34$). Pentameric FITC−WT-PLB labeled at a high concentration (200 μM) exhibited a decreased anisotropy compared to that of the monomer ($r = 0.25$), suggesting depolarization by homoFRET. However, the WT-PLB−FITC pentamer underlabeled with 10 μM FITC exhibited high anisotropy ($r = 0.4$), indicating null homotransfer (not shown). These observations are in harmony with measurements made with FlAsH-labeled tetracysPLB.

The FRET origin of the observed depolarization of pentamer emission was confirmed by excising the pentamer band of FlAsH−IB-tetracysPLB from the gel and heating it with a custom cuvette thermocontroller apparatus, with continuous measurement of fluorescence anisotropy. As the temperature is increased, there is an initial decrease in anisotropy due to increased probe mobility and decreased solvent viscosity (Figure 13, phase 1) followed by melting of the pentamer and loss of FRET, evident as an abrupt increase in fluorescence anisotropy (Figure 13, phase 2). Furthermore, reducing the number of fluorescent labels by photobleaching of FlAsH-labeled IB-tetracysPLB pentamer with intense 498.5 nm illumination from an argon laser caused a progressive increase in pentamer fluorescence anisotropy (Figure 14, blue points and regression) that approached the monomer (null homotransfer) value. The Runnels et al. generalization (*41*) of the Knox cluster theory

Table 2: Construct Fluorescence Anisotropy Values, Calculated Transfer Distances, and Predicted Probe Separations for Three Tetracysteine PLB Mutants

	anisotropy	R (Å)	predicted from model
N-term-tetracysPLB monomer	0.29		
N-term-tetracysPLB pentamer	0.21	46.1 ± 2.1	46.7
IA-tetracysPLB monomer	0.29		
IA-tetracysPLB pentamer	0.17	37.9 ± 3.8	39.1
IB-tetracysPLB monomer	0.29		
IB-tetracysPLB pentamer	0.11	<25	20.6

(*42*) simplifies to $r \propto 1/N$ at short transfer distances ($R_0 \gg R$). Anisotropy is inversely and linearly related to stoichiometry, and thus to the total remaining fluorescence in this experiment. A negative control IB-tetracysPLB pentamer underlabeled with 5 μM FlAsH had one fluorophore per pentamer or fewer before photobleaching had begun. Consequently, it exhibited high fluorescence anisotropy, unchanged by photobleaching (Figure 13, red points and regression).

DISCUSSION

Heterotransfer FRET experiments with two biarsenical probe color variants, FlAsH and ReAsH, showed intrapentameric energy transfer occurs in vitro (Figures 5 and 6) and in vivo (Figure 7). We observed a graduated pattern of FlAsH donor fluorescence quenching by the ReAsH acceptor for PLB constructs bearing tetra-Cys repeats at different points along their primary sequence (Figure 4). Construct IB, labeled in the juxtamembrane region, showed the greatest quenching of FlAsH fluorescence when colabeled with ReAsH, while N-term, with a tetra-Cys repeat on an N-terminal extension, was quenched the least. Construct IA, labeled in the middle of the cytoplasmic domain, was quenched to an intermediate degree. We conclude that as the labeling site is moved away from the transmembrane domain and toward the N-terminus, the extent of energy transfer is decreased. These results are qualitatively interesting, but difficult to quantitatively calibrate to probe separation distances because of the unknown donor:acceptor:protein molar ratio. We therefore examined FlAsH−FlAsH energy transfer, that is, homotransfer. FRET between spectrally identical fluorophores has been utilized for assessment of oligomerization (*44*, *53*, *54*) and probe separation distance (*45*). The efficacy of polarization macroscopy for detecting homotransfer FRET in a polyacrylamide gel was established using BSA labeled at different dye:protein ratios (Figure 8). In-gel fluorescence anisotropy of pentamers composed of N-term-, IA-, and IB-tetracysPLB indicated a graduated pattern of depolarization (Figure 10). Photobleaching (Figure 14) and heat disruption of the pentamer (Figure 13) confirm that fluorescence resonance energy homotransfer is the source of the observed depolarization. Similar results were obtained with wild-type phospholamban labeled on Lys3 with FITC (Figure 12). Using a generalization (*41*) of the Knox cluster theory (*42*), we determined the probe separation distance for each construct, shown in Table 2. Data are mean ± SE for six experiments.

FRET efficiency is nearly unity for all distances of <25 Å; thus, the transfer radius (R) for IB-tetracysPLB can only be described as being below this limit. The results are in

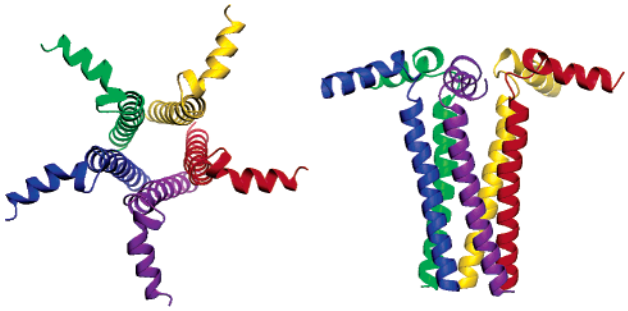

FIGURE 15: Model of the phospholamban pentamer.

harmony with the heterotransfer results, and suggest that the probe separation distance is greatest at the N-termini of the PLB pentamer cytoplasmic domains; that is, the domains flare away from one another with axial declination toward the membrane surface, as proposed by Pollesello et al. (*27*). The cytoplasmic domain axial angle exceeds previous estimates from FTIR measurements (*55*). Instead, the present data are compatible with the recent observation that a spin probe directed to position 11 of a monomeric mutant of PLB was relaxed by Ni^{2+} chelated by lipid headgroups, indicating a population of PLB in direct contact with the membrane surface (*56*). Our FRET measurements are not consistent with the subunits being parallel α-helices normal to the membrane surface, as suggested previously (*25*, *26*). One would expect subunits arranged in a continuous coiled coil to display uniform, short radius energy transfer regardless of the labeling position. The transfer distances determined here compare favorably with a model of pentameric PLB derived from the monomeric PLB NMR structural information (*49*) (Figure 15). The labeling site separation distances predicted from this model were 46.7, 39.1, and 20.6 Å for N-term, IA, and IB, respectively (Table 2).

The Runnels and Scarlatta adaptation (*41*) of the Knox cluster theory (*42*) assumes uncorrelated donor and acceptor fluorescence transition dipoles. The contrary case of a correlated donor and acceptor may be considered by analogy to a single fluorophore with displaced absorption and emission dipoles, in which fluorescence is depolarized by a factor $(3\cos^2\theta_T - 1)/2$, where θ_T is the angle between the absorption and emission transition moments. This effect is a concern for oriented probes bound to a macromolecular complex of defined geometry. However, dipole correlation is reduced by attachment flexibility of the FlAsH probe and by axial and azimuthal dynamics of the PLB cytoplasmic domain. While the bidentate attachment of FlAsH to tetra-Cys repeats constrains probe orientation and mobility (*36*), we detect some fast (nanosecond) disorder that gives a monomer fluorescence anisotropy of 0.29. This corresponds to a probe order parameter (S) of 0.85 by $(r/r_0)^{1/2}$, where the limiting anisotropy $r_0 = 0.4$. An order parameter of 0.85 represents a wobble cone half-angle (θ_C) of 26° according to the relationship $\theta_C = \cos^{-1}[-0.5 + 0.5(1 + 8S)^{1/2}]$. The randomization of probes by dynamic disorder can be conservatively estimated from the order parameter as a set of upper and lower bounds for κ^2 (*57*, *58*) according to the equations $\kappa^2_{min} = {}^2/_3[1 - (S_D + S_A)/2)]$ and $\kappa^2_{max} = {}^2/_3(1 + S_D + S_A + 3S_DS_A)$. When $S = 0.85$, κ^2 for a given donor/acceptor pair may be as low as 0.1 or as high as 3.25, which implies a maximum uncertainty of R_0 of 30%. However, there is likely to be some additional heterogeneity that is "static" in the sense that it occurs over a time scale not detected during the nanosecond lifetime of FlAsH. For example, recent results show multiple populations of monomeric PLB with distinguishable dynamics characteristics (*59*). We conclude that the combined dynamic (nanosecond) and static (microsecond or slower) disorder justifies approximating the mutual orientation of the donor and acceptor fluorescence dipoles as uncorrelated, as in Runnels et al. (*41*).

FlAsH complexed to peptides has been reported to have picomolar affinity, with dissociation kinetics on the order of several weeks (*36*). Consistent with this, we have observed that excised gel slices of the labeled PLB pentamer retain high fluorescence and low anisotropy after several days. Dissociation rates on a time scale comparable to that of electrophoresis would result in blurred bands smeared at their leading edge, but we consistently observed clean protein bandfronts.

Fluorescein has been observed to self-quench at high concentrations (*60*), resulting in increased anisotropy. This is probably not a significant factor in this study, since heterotransfer efficiencies (Figure 4) for the three derivatized tetracysteine constructs qualitatively parallel homotransfer results (Figure 10). In addition, self-quenching would be expected to worsen (increasing anisotropy) at higher dye:protein ratios. Instead, we found that fluorescence increased and anisotropy decreased with an increase in labeling stoichiometry (not shown), and fluorescence decreased and anisotropy increased with photobleaching (Figure 14). These observations are consistent with greater depolarization by homoFRET at higher dye:protein ratios.

Our study demonstrates the effectiveness of investigating protein−protein interactions and quaternary conformation by assessing fluorescence resonance energy transfer in an electrophoresis gel. This inexpensive approach may be extended to nondenaturing conditions, and offers several unique advantages. It is a high-throughput technique, in that multiple samples in parallel lanes and multiple species within a lane are all evaluated simultaneously. It is well suited to studying solvent effects; by soaking the entire gel in multiple successive buffer solutions, one may investigate the effects of pH and ionic strength on the same protein samples. It is internally controlled for spurious signals, such as highly polarized scattered light, which is subtracted as background. Most importantly for this work, electrophoresis affects spatial separation of various fluorescent species that would otherwise be impossible to resolve, including phospholamban monomers and pentamers, higher-order and intermediate-order oligomers, unincorporated fluorescent dye, and endogenous Cys-containing proteins that have been labeled with FlAsH (*61*).

SUMMARY

In-gel macroscopy measurements of phospholamban pentamer fluorescence anisotropy suggest differential energy transfer efficiencies for three labeling sites on the PLB cytoplasmic domain. This implies that the probe separation distances are graduated by position along the PLB primary sequence, consistent with a helical pinwheel pentamer conformation in which the N-termini flare away from one another with axial declination toward the membrane surface.

ACKNOWLEDGMENT

We thank Jerry Sedgewick and John Oja for assistance with the construction of the in-gel anisotropy setup, Igor Negrashov for building the cuvette thermocontroller apparatus, and Mike Autry, Deb Winters, and Sarah Blakely for help with molecular biology and protein expression. Plasmid pGEX-PLB was provided by Tara L. Kirby. Thanks to M. G. Paterlini for advice on PLB pentamer molecular modeling. We are grateful to Yuk Yin Sham and the University of Minnesota Supercomputing Institute (MSI) for technical assistance with modeling, and for the use of MSI computing resources. Gianluigi Veglia provided advice about the use of NMR structural data. FlAsH was kindly provided by Roger Cooke.

REFERENCES

1. James, P., Inui, M., Tada, M., Chiesi, M., and Carafoli, E. (1989) Nature and site of phospholamban regulation of the Ca2+ pump of sarcoplasmic reticulum, *Nature 342*, 90−92.
2. Kim, H. W., Steenaart, N. A., Ferguson, D. G., and Kranias, E. G. (1990) Functional reconstitution of the cardiac sarcoplasmic reticulum Ca^{2+}-ATPase with phospholamban in phospholipid vesicles, *J. Biol. Chem. 265*, 1702−1709.
3. Kranias, E. G. (1985) Regulation of calcium transport by protein phosphatase activity associated with cardiac sarcoplasmic reticulum, *J. Biol. Chem. 260*, 11006−11010.
4. Simmerman, H. K., Collins, J. H., Theibert, J. L., Wegener, A. D., and Jones, L. R. (1986) Sequence analysis of phospholamban. Identification of phosphorylation sites and two major structural domains, *J. Biol. Chem. 261*, 13333−13341.
5. Tada, M., Inui, M., Yamada, M., Kadoma, M., Kuzuya, T., Abe, H., and Kakiuchi, S. (1983) Effects of phospholamban phosphorylation catalyzed by adenosine 3′:5′-monophosphate- and calmodulin-dependent protein kinases on calcium transport ATPase of cardiac sarcoplasmic reticulum, *J. Mol. Cell. Cardiol. 15*, 335−346.
6. Minamisawa, S., Hoshijima, M., Chu, G., Ward, C. A., Frank, K., Gu, Y., Martone, M. E., Wang, Y., Ross, J., Jr., Kranias, E. G., Giles, W. R., and Chien, K. R. (1999) Chronic phospholamban-sarcoplasmic reticulum calcium ATPase interaction is the critical calcium cycling defect in dilated cardiomyopathy, *Cell 99*, 313−322.
7. Sande, J. B., Sjaastad, I., Hoen, I. B., Bokenes, J., Tonnessen, T., Holt, E., Lunde, P. K., and Christensen, G. (2002) Reduced level of serine(16) phosphorylated phospholamban in the failing rat myocardium: A major contributor to reduced SERCA2 activity, *Cardiovasc. Res. 53*, 382−391.
8. Haghighi, K., Kolokathis, F., Pater, L., Lynch, R. A., Asahi, M., Gramolini, A. O., Fan, G. C., Tsiapras, D., Hahn, H. S., Adamopoulos, S., Liggett, S. B., Dorn, G. W., II, MacLennan, D. H., Kremastinos, D. T., and Kranias, E. G. (2003) Human phospholamban null results in lethal dilated cardiomyopathy revealing a critical difference between mouse and human, *J. Clin. Invest. 111*, 869−876.
9. Schmidt, A. G., Edes, I., and Kranias, E. G. (2001) Phospholamban: A promising therapeutic target in heart failure? *Cardiovasc. Drugs Ther. 15*, 387−396.
10. Hoshijima, M., Ikeda, Y., Iwanaga, Y., Minamisawa, S., Date, M. O., Gu, Y., Iwatate, M., Li, M., Wang, L., Wilson, J. M., Wang, Y., Ross, J., Jr., and Chien, K. R. (2002) Chronic suppression of heart-failure progression by a pseudophosphorylated mutant of phospholamban via in vivo cardiac rAAV gene delivery, *Nat. Med. 8*, 864−871.
11. Minino, A. M., and Smith, B. L. (2001) Deaths: Preliminary Data for 2000, *National Vital Statistics Report*, Vol. 49, Centers for Disease Control and Prevention, Atlanta.
12. Wegener, A. D., and Jones, L. R. (1984) Phosphorylation-induced mobility shift in phospholamban in sodium dodecyl sulfate-polyacrylamide gels. Evidence for a protein structure consisting of multiple identical phosphorylatable subunits, *J. Biol. Chem. 259*, 1834−1841.
13. Simmerman, H. K. B., Kobayashi, Y. M., Autry, J. M., and Jones, L. R. (1996) A Leucine Zipper Stabilizes the Pentameric Membrane Domain of Phospholamban and Forms a Coiled-coil Pore Structure, *J. Biol. Chem. 271*, 5941−5946.
14. Thomas, D. D., Reddy, L. G., Karim, C. B., Li, M., Cornea, R., Autry, J. M., Jones, L. R., and Stamm, J. (1998) Direct spectroscopic detection of molecular dynamics and interactions of the calcium pump and phospholamban, *Ann. N.Y. Acad. Sci. 853*, 186−194.
15. Karim, C. B., Stamm, J. D., Karim, J., Jones, L. R., and Thomas, D. D. (1998) Cysteine reactivity and oligomeric structures of phospholamban and its mutants, *Biochemistry 37*, 12074−12081.
16. Cornea, R. L., Autry, J. M., Chen, Z., and Jones, L. R. (2000) Reexamination of the role of the leucine/isoleucine zipper residues of phospholamban in inhibition of the Ca^{2+} pump of cardiac sarcoplasmic reticulum, *J. Biol. Chem. 275*, 41487−41494.
17. Wegener, A. D., Simmerman, H. K., Lindemann, J. P., and Jones, L. R. (1989) Phospholamban phosphorylation in intact ventricles. Phosphorylation of serine 16 and threonine 17 in response to β-adrenergic stimulation, *J. Biol. Chem. 264*, 11468−11474.
18. Reddy, L. G., Jones, L. R., Cala, S. E., O'Brian, J. J., Tatulian, S. A., and Stokes, D. L. (1995) Functional reconstitution of recombinant phospholamban with rabbit skeletal Ca^{2+}-ATPase, *J. Biol. Chem. 270*, 9390−9397.
19. Kimura, Y., Kurzydlowski, K., Tada, M., and MacLennan, D. H. (1997) Phospholamban inhibitory function is activated by depolymerization, *J. Biol. Chem. 272*, 15061−15064.
20. Zhai, J., Schmidt, A. G., Hoit, B. D., Kimura, Y., MacLennan, D. H., and Kranias, E. G. (2000) Cardiac-specific overexpression of a superinhibitory pentameric phospholamban mutant enhances inhibition of cardiac function in vivo, *J. Biol. Chem. 275*, 10538−10544.
21. Zvaritch, E., Backx, P. H., Jirik, F., Kimura, Y., de Leon, S., Schmidt, A. G., Hoit, B. D., Lester, J. W., Kranias, E. G., and MacLennan, D. H. (2000) The transgenic expression of highly inhibitory monomeric forms of phospholamban in mouse heart impairs cardiac contractility, *J. Biol. Chem. 275*, 14985−14991.
22. Cornea, R. L., Jones, L. R., Autry, J. M., and Thomas, D. D. (1997) Mutation and phosphorylation change the oligomeric structure of phospholamban in lipid bilayers, *Biochemistry 36*, 2960−2967.
23. Reddy, L. G., Jones, L. R., and Thomas, D. D. (1999) Depolymerization of phospholamban in the presence of calcium pump: A fluorescence energy transfer study, *Biochemistry 38*, 3954−3962.
24. Li, M., Reddy, L. G., Bennett, R., Silva, N. D., Jr., Jones, L. R., and Thomas, D. D. (1999) A fluorescence energy transfer method for analyzing protein oligomeric structure: Application to phospholamban, *Biophys. J. 76*, 2587−2599.
25. Arkin, I. T., Rothman, M., Ludlam, C. F., Aimoto, S., Engelman, D. M., Rothschild, K. J., and Smith, S. O. (1995) Structural model of the phospholamban ion channel complex in phospholipid membranes, *J. Mol. Biol. 248*, 824−834.
26. Smith, S. O., Kawakami, T., Liu, W., Ziliox, M., and Aimoto, S. (2001) Helical structure of phospholamban in membrane bilayers, *J. Mol. Biol. 313*, 1139−1148.
27. Pollesello, P., Annila, A., and Ovaska, M. (1999) Structure of the 1−36 amino-terminal fragment of human phospholamban by nuclear magnetic resonance and modeling of the phospholamban pentamer, *Biophys. J. 76*, 1784−1795.
28. Wegener, A. D., Simmerman, H. K., Liepnieks, J., and Jones, L. R. (1986) Proteolytic cleavage of phospholamban purified from canine cardiac sarcoplasmic reticulum vesicles. Generation of a low resolution model of phospholamban structure, *J. Biol. Chem. 261*, 5154−5159.
29. Li, M., Cornea, R. L., Autry, J. M., Jones, L. R., and Thomas, D. D. (1998) Phosphorylation-induced structural change in phospholamban and its mutants, detected by intrinsic fluorescence, *Biochemistry 37*, 7869−7877.
30. Wegener, A. D., and Jones, L. R. (1984) Phosphorylation-induced mobility shift in phospholamban in sodium dodecyl sulfate-polyacrylamide gels. Evidence for a protein structure consisting of multiple identical phosphorylatable subunits, *J. Biol. Chem. 259*, 1834−1841.
31. Simmerman, H. K., Lovelace, D. E., and Jones, L. R. (1989) Secondary structure of detergent-solubilized phospholamban, a phosphorylatable, oligomeric protein of cardiac sarcoplasmic reticulum, *Biochim. Biophys. Acta 997*, 322−329.
32. Lockwood, N. A., Tu, R. S., Zhang, Z., Tirrell, M. V., Thomas, D. D., and Karim, C. B. (2003) Structure and function of integral membrane protein domains resolved by peptide-amphiphiles: Application to phospholamban, *Biopolymers 69*, 283−292.

33. Griffin, B. A., Adams, S. R., and Tsien, R. Y. (1998) Specific covalent labeling of recombinant protein molecules inside live cells, *Science 281*, 269−272.
34. Gaietta, G., Deerinck, T. J., Adams, S. R., Bouwer, J., Tour, O., Laird, D. W., Sosinsky, G. E., Tsien, R. Y., and Ellisman, M. H. (2002) Multicolor and electron microscopic imaging of connexin trafficking, *Science 296*, 503−507.
35. Buck, B., Zamoon, J., Kirby, T. L., DeSilva, T. M., Karim, C., Thomas, D., and Veglia, G. (2003) Overexpression, purification, and characterization of recombinant Ca-ATPase regulators for high-resolution solution and solid-state NMR studies, *Protein Expression Purif. 30*, 253−261.
36. Adams, S. R., Campbell, R. E., Gross, L. A., Martin, B. R., Walkup, G. K., Yao, Y., Llopis, J., and Tsien, R. Y. (2002) New biarsenical ligands and tetracysteine motifs for protein labeling in vitro and in vivo: Synthesis and biological applications, *J. Am. Chem. Soc. 124*, 6063−6076.
37. Autry, J. M., and Jones, L. R. (1997) Functional co-expression of the canine cardiac Ca^{2+} pump and phospholamban in *Spodoptera frugiperda* (Sf21) cells reveals new insights on ATPase regulation, *J. Biol. Chem. 272*, 15872−15880.
38. Ferrington, D. A., Yao, Q., Squier, T. C., and Bigelow, D. J. (2002) Comparable levels of Ca-ATPase inhibition by phospholamban in slow-twitch skeletal and cardiac sarcoplasmic reticulum, *Biochemistry 41*, 13289−13296.
39. Mayer, E. J., McKenna, E., Garsky, V. M., Burke, C. J., Mach, H., Middaugh, C. R., Sardana, M., Smith, J. S., and Johnson, R. G., Jr. (1996) Biochemical and biophysical comparison of native and chemically synthesized phospholamban and a monomeric phospholamban analog, *J. Biol. Chem. 271*, 1669−1677.
40. Förster, T. (1948) Intermolecular energy migration and fluorescence, *Ann. Phys. 2*, 55−75.
41. Runnels, L. W., and Scarlata, S. F. (1995) Theory and application of fluorescence homotransfer to melittin oligomerization, *Biophys. J. 69*, 1569−1583.
42. Knox, R. S. (1968) Theory of polarization quenching by excitation transfer, *Physica 39*, 361−386.
43. Griffin, B. A., Adams, S. R., Jones, J., and Tsien, R. Y. (2000) Fluorescent labeling of recombinant proteins in living cells with FlAsH, *Methods Enzymol. 327*, 565−578.
44. Rocheleau, J. V., Edidin, M., and Piston, D. W. (2003) Intrasequence GFP in class I MHC molecules, a rigid probe for fluorescence anisotropy measurements of the membrane environment, *Biophys. J. 84*, 4078−4086.
45. Lillo, M. P., Canadas, O., Dale, R. E., and Acuna, A. U. (2002) Location and properties of the taxol binding center in microtubules: A picosecond laser study with fluorescent taxoids, *Biochemistry 41*, 12436−12449.
46. Moens, P. D., Helms, M. K., and Jameson, D. M. (2004) Detection of tryptophan to tryptophan energy transfer in proteins, *Protein J. 23*, 79−83.
47. Jameson, D. M., Croney, J. C., and Moens, P. D. (2003) Fluorescence: Basic concepts, practical aspects, and some anecdotes, *Methods Enzymol. 360*, 1−43.
48. Galanin, M. (1950) *Tr. Fiz. Inst. I. P. Pavlova 5*, 341.
49. Zamoon, J., Mascioni, A., Thomas, D. D., and Veglia, G. (2003) NMR solution structure and topological orientation of monomeric phospholamban in dodecylphosphocholine micelles, *Biophys. J. 85*, 2589−2598.
50. LaConte, L. E., Voelz, V., Nelson, W., Enz, M., and Thomas, D. D. (2002) Molecular dynamics simulation of site-directed spin labeling: Experimental validation in muscle fibers, *Biophys. J. 83*, 1854−1866.
51. Koradi, R., Billeter, M., and Wuthrich, K. (1996) MOLMOL: A program for display and analysis of macromolecular structures, *J. Mol. Graphics 14*, 51−55, 29−32.
52. Ono, M., Murakami, T., Kudo, A., Isshiki, M., Sawada, H., and Segawa, A. (2001) Quantitative comparison of anti-fading mounting media for confocal laser scanning microscopy, *J. Histochem. Cytochem. 49*, 305−312.
53. Gautier, I., Tramier, M., Durieux, C., Coppey, J., Pansu, R. B., Nicolas, J. C., Kemnitz, K., and Coppey-Moisan, M. (2001) Homo-FRET microscopy in living cells to measure monomer−dimer transition of GFP-tagged proteins, *Biophys. J. 80*, 3000−3008.
54. Lidke, D. S., Nagy, P., Barisas, B. G., Heintzmann, R., Post, J. N., Lidke, K. A., Clayton, A. H., Arndt-Jovin, D. J., and Jovin, T. M. (2003) Imaging molecular interactions in cells by dynamic and static fluorescence anisotropy (rFLIM and emFRET), *Biochem. Soc. Trans. 31*, 1020−1027.
55. Tatulian, S. A., Jones, L. R., Reddy, L. G., Stokes, D. L., and Tamm, L. K. (1995) Secondary structure and orientation of phospholamban reconstituted in supported bilayers from polarized attenuated total reflection FTIR spectroscopy, *Biochemistry 34*, 4448−4456.
56. Kirby, T. L., Karim, C. B., and Thomas, D. D. (2004) Electron paramagnetic resonance reveals a large-scale conformational change in the cytoplasmic domain of phospholamban upon binding to the sarcoplasmic reticulum Ca-ATPase, *Biochemistry 43*, 5842−5852.
57. Dale, R. E., Eisinger, J., and Blumberg, W. E. (1979) The orientational freedom of molecular probes. The orientation factor in intramolecular energy transfer, *Biophys. J. 26*, 161−193.
58. Lakowicz, J. R., Gryczynski, I., Cheung, H. C., Wang, C. K., Johnson, M. L., and Joshi, N. (1988) Distance distributions in proteins recovered by using frequency-domain fluorometry. Applications to troponin I and its complex with troponin C, *Biochemistry 27*, 9149−9160.
59. Karim, C. B., Kirby, T. L., Zhang, Z., Nesmelov, Y. E., and Thomas, D. D. (2004) Phospholamban structural dynamics in lipid bilayers probed by a spin label rigidly coupled to the peptide backbone, *Proc. Natl. Acad. Sci. U.S.A.* (in press).
60. Kawski, A. (1983) Excitation energy transfer and its manifestation in isotropic media, *Photochem. Photobiol. 38*, 487−508.
61. Stroffekova, K., Proenza, C., and Beam, K. G. (2001) The protein-labeling reagent FLASH-EDT2 binds not only to CCXXCC motifs but also non-specifically to endogenous cysteine-rich proteins, *Pfluegers Arch. 442*, 859−866.

BI0478446